Journal of Power Sources 384 (2018) 328–333

Contents lists available at ScienceDirect

Journal of Power Sources

journal homepage: www.elsevier.com/locate/jpowsour

A high-performance ternary Si composite anode material with crystal graphite core and amorphous carbon shell

Dong Sui[a], Yuqing Xie[a], Weimin Zhao[b], Hongtao Zhang[a], Ying Zhou[a], Xiting Qin[a], Yanfeng Ma[a], Yong Yang[b,**], Yongsheng Chen[a,*]

[a] The Centre of Nanoscale Science and Technology and Key Laboratory of Functional Polymer Materials, State Key Laboratory and Institute of Elemento-Organic Chemistry, College of Chemistry, Nankai University, Tianjin 300071, China

[b] State Key Laboratory for Physical Chemistry of Solid Surfaces, Collaborative Innovation Center of Chemistry for Energy Materials (iChEM), Department of Chemistry, College of Chemistry and Chemical Engineering, Xiamen University, Xiamen 361005, China

HIGHLIGHTS

- A ternary core/shell Si/graphite/pyrolytic carbon composite was prepared.
- Over 80% capacity retention was obtained after 300 cycles.
- High performance benefits from the peculiar structure of the composite.

GRAPHICAL ABSTRACT

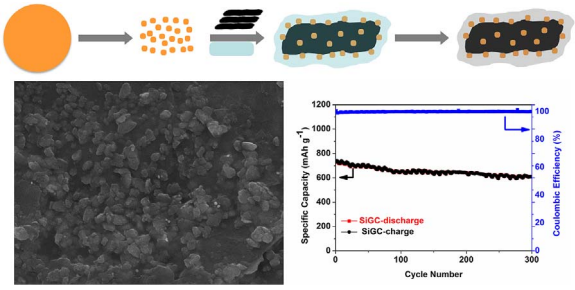

ARTICLE INFO

Keywords:
Lithium ion battery
Si
Ternary composite
Anode material
Industry process

ABSTRACT

Si is a promising anode material for lithium-ion batteries, but suffers from sophisticated engineering structures and complex fabrication processes that pose challenges for commercial application. Herein, a ternary Si/graphite/pyrolytic carbon (SiGC) anode material with a structure of crystal core and amorphous shell using low-cost raw materials is developed. In this ternary SiGC composite, Si component exists as nanoparticles and is spread on the surface of the core graphite flakes while the sucrose-derived pyrolytic carbon further covers the graphite/Si components as the amorphous shell. With this structure, Si together with the graphite contributes to the high specific capacity of this Si ternary material. Also the graphite serves as the supporting and conducting matrix and the amorphous shell carbon could accommodate the volume change effect of Si, reinforces the integrity of the composite architecture, and prevents the graphite and Si from direct exposing to the electrolyte. The optimized ternary SiGC composite displays high reversible specific capacity of 818 mAh g^{-1} at 0.1 A g^{-1}, initial Coulombic efficiency (CE) over 80%, and excellent cycling stability at 0.5 A g^{-1} with 83.6% capacity retention (~610 mAh g^{-1}) after 300 cycles.

1. Introduction

In recent years, with the fast development of electric vehicles and portable electronics, lithium-ion batteries (LIBs) with higher energy density and better cycling performance are highly demanded and extensive efforts have been made to search for new cathode and anode

* Corresponding author.
** Corresponding author.
E-mail addresses: yyang@xmu.edu.cn (Y. Yang), yschen99@nankai.edu.cn (Y. Chen).

https://doi.org/10.1016/j.jpowsour.2018.03.008
Received 28 November 2017; Received in revised form 7 February 2018; Accepted 4 March 2018

materials with higher specific capacity [1–5]. For LIBs anode materials, graphite, which has dominated current commercial anode market for nearly three decades, suffers a relatively low capacity and safety problems. Among the potential anode candidates, Si-based anode materials are one of the most promising ones due to its extremely high specific capacity (3580 mAh g^{-1} vs. 372 mAh g^{-1} for graphite), abundant resource, and proper lithium-alloy potential (0.2 V vs. Li^+/Li) [6,7]. In spite of these superior advantages, the practical application of Si-based materials, especially bulk Si, is still severely hindered by some drawbacks, such as huge volume variation during lithium alloy/de-alloy, continues formation of solid electrolyte interface (SEI), and low intrinsic electric and ion conductivity [8]. To address these critical issues, several strategies have been successfully developed, including designing nano-Si structure, introducing carbon-buffering layer, and optimizing the choice of binder and electrolyte [9–14]. A variety of Si-based nano-materials, e.g. nanoparticles, nanowires, nanotubes, and core/shell nanostructures, show better electrochemical performance than pure bulk Si [7,12,15–19]. However, considering the cost, scalability, energy consumption and pollution, these strategies are rather hard to achieve commercial applications. Therefore, it is highly desirable to develop low-cost and scalable strategies to prepare Si-based anode materials with high capacity and cycling stability.

Fabricating Si/C composites are efficient approaches to circumvent the limitations of pure Si by introducing graphite and/or amorphous carbon, thus improving their electrochemical performance [12,14,20–26]. These carbon components not only enhance the conductivity of the composites, but also suppress the huge volume variation of Si, keep the integrity of electrode, and prevent direct contact of Si with the electrolyte. Herein, we developed a ternary Si/graphite/pyrolytic carbon (SiGC) composite with a structure of crystal core (graphite) and amorphous shell (sucrose derived pyrolytic carbon) by easy and scalable ball milling and spray drying process. The optimized SiGC composite with Si content of 12.8 wt% displays high initial reversible specific capacity of 818 mAh g^{-1} at 0.1 A g^{-1} and long cycle life up to 300 cycles at 0.5 A g^{-1} with 83.6% capacity retention. Moreover, high initial CE (over 80%) as well as good rate capability was achieved. Such super performance should be ascribed to the peculiar structure of the ternary SiGC composite and synergistic effect of the three components.

2. Experimental section

2.1. Synthesis of ternary SiGC composite with crystal core and amorphous shell

All the starting materials are commercially available low-cost products. Different mass ratio of Si, graphite and sucrose (1:4:5, 1:7:5, 1:10:5) were fabricated for systematic studies. Here is the typical synthesis process for the ternary SiGC composite with crystal core and amorphous shell. First, micro-sized Si powder with particle size of about 10 μm (1000 g, Xuzhou Lingyun Silicon Industry Co. Ltd.) was ball-milled in alcohol (3000 g) with Zirconia beads (0.1 mm diameter) for 8 h at 60 Hz via wet grinding (Labstar LMZ, Netzsch). Then, the as-obtained suspension (25 wt%, 200 g) of nano-Si in alcohol was mixed with graphite (350 g, Huaxin Energy Material Co. Ltd.), sucrose (250 g) and water (1180 g) by ball milling for 30 min at 30 Hz. The overall solid content of the mixture was adjusted to 30 wt%. After that, the resulting homogeneous suspension was spray dried with inlet temperature of 140 °C and outlet temperature of 80 °C at a rate of 1000 mL/h in a spray dryer (Shanghai Pilotech Instrument Equipment Co. Ltd.). Finally, the spray-dried solid precursor was calcined at 800 °C for 2 h under H_2/Ar (5:95 v/v) atmosphere at a heating rate of 5 °C min^{-1} to obtain the SiGC composite. For comparison, binary Si/graphite (SiG) composite without amorphous pyrolytic carbon shell was also prepared by similar procedure.

2.2. Material characterization

Thermogravimetric (TG) measurement (Netzsch-STA 449C) was conducted from room temperature to 900 °C at a heating rate of 10 °C min^{-1} in air. Powder X-ray diffraction (XRD) analysis was performed on a Rigaku D/Max-2500 diffractometer with Cu Kα radiation. Raman spectra were recorded using a Lab RAM HR Evolution with a 514.5 nm Ar-ion laser. Scanning electron microscopy (SEM) was carried out using a LEO 1530 VP field emission scanning electron microscope with an acceleration voltage of 10 kV. Transmission electron microscopy (TEM) as performed using a JEOL TEM-2100 electron microscope operated at 200 kV.

2.3. Cell fabrication and electrochemical measurements

Electrochemical performances were characterized using coin-type cells. To prepare working electrodes, the active materials, Super P carbon black, and poly(vinylidene fluoride) (5 wt% in N-methyl-2-pyrrolidone) were mixed with a mass ratio of 80:10:10 to produce a homogenous slurry which was then coated onto a Cu foil (10 μm in thickness) with areal density of about 1.1 mg cm^{-2}. After heating at 60 °C for 3 h and 150 °C for 1 h, the electrode sheet was punched into 11 mm diameter electrodes and then pressed under pressure of 10 MPa. The coin-type cells were assembled in an argon-filled glove box with lithium metal foil as the counter/reference electrode. The electrolyte was 1 M $LiPF_6$ in ethylene carbonate/diethyl carbonate/vinylene carbonate (1:1:0.02 v/v/v). The galvanostatic charge/discharge cycles were performed in the voltage window of 0.01–1.5 V at 25 °C using a battery test system (LAND CT2001A model, Wuhan LAND Electronics. Ltd.). Electrochemical impedance spectra (EIS) measurements were recorded using an Autolab system (Metrohm). The EIS measurements were carried out at AC amplitude of 10 mV in the frequency range from 100 kHz to 10 mHz.

3. Results and discussion

3.1. Structure and morphology

To synthesis the ternary SiGC composite with a peculiar core/shell structure, we developed a simple approach as shown in Fig. 1 and the

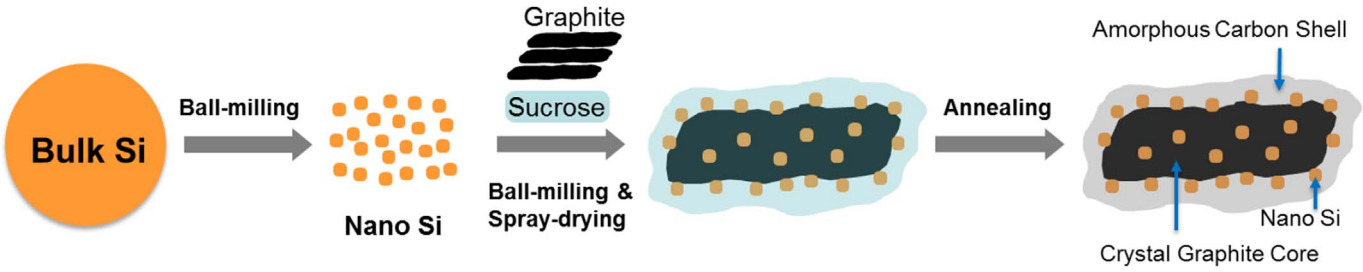

Fig. 1. Schematic of the synthesis process of the SiGC composite.

details of the preparation process is presented in the Experimental section 2.1. Industry bulk Si powder, graphite and sucrose were used directly as the starting materials. To control the Si morphology and achieve better performance, the grey bulk Si was first ball-milled to nano size particles. After that, the nano-scaled Si was further ball-milled with graphite (carbon source for the crystal core) and sucrose (carbon source for the amorphous shell) to achieve the state where the nano-Si should be dispersed on the surface of graphite and coated with sucrose. Then the material was heat treated and the original sucrose coating on the nano-Si and graphite should be converted to amorphous carbon and the ternary SiGC composite with a structure of crystal core and amorphous shell was obtained. It is important to note that our ternary Si-based composite was started with the cheap raw materials. Furthermore, ball-milling and spray-drying are simple and industrial-scale preparation process. As a result, the obtained SiGC product with high performance prepared by our strategy is cost-effective for practical application.

Thermogravimetric analysis results in air for ball-milled Si, the compared binary SiG (Si and graphite only, without being coated by amorphous carbon shell), and SiGC (with different Si content) were shown in Fig. 2a and Fig. S1. It can be seen that the TGA test in air up to 900 °C indicate the sample weight of bare nano silicon increases to 111.5% due to the oxidation. With this data, from the TG curves, the Si contents in SiG and SiGC (1:7:5) could be determined to be around 10.5 wt% and 12.8 wt%, respectively [21,22]. For SiGC, the decomposition of sucrose-derived amorphous carbon mainly takes place below 650 °C, while the weight loss of crystal core of graphiteis over 650 °C. Fig. 2b shows the compared XRD patterns of the SiGC, SiG, graphite and ball-milled nano-Si intermediate products. The typical peaks of graphite and silicon in the SiGC and SiG composites are identical with graphite and ball-milled Si nanoparticles correspondingly. The strong peak at 26.5° belongs to diffraction plane of (002) of graphite while the peaks at 28.4°, 47.3°, 56.1° can be assigned to the typical diffraction planes of (111), (220), (311) for silicon, respectively [27]. These results illustrate that the crystalline of graphite and silicon in the SiGC and SiG are well kept and no impurity was observed. Furthermore, the Raman spectra of SiGC, SiG, graphite and ball-milled Si nanoparticles are demonstrated in Fig. 2c. The peaks of the silicon nanoparticles and graphite in the SiGC and SiG are well consistent with its precursors. Specifically, the sharp peak at 515 cm^{-1} observed in the SiGC and SiG composites is assigned to crystalline Si and is well matched with ball-milled silicon nanoparticles, while there are two peaks located at 1572 and 2726 cm^{-1}corresponding to G-band and 2D band of graphite respectively [27,28]. Compared with the pristine graphite and binary SiG, the peak at 1356 cm^{-1} (D band caused by disordered carbon) of SiGC is much stronger and is ascribed to the sucrose-derived amorphous carbon shell coated on the surface of silicon nanoparticles and graphite.

The morphology and microstructure of SiGC, SiG, and their precursors were characterized by SEM and TEM. Fig. 3a and Fig. S2a shows the typical SEM image of the ball-milled nano-sized Si and the pristine bulk Si, indicating that most micro-sized raw silicon was ground to nanoscaled particles. As demonstrated in Fig. S2b, the micro-sized flake-shaped pristine graphite could serve as the surporter and conducting matrix for nano-Si. In Fig. 3b and c, it can be clearly observed that ball-milled Si nanoparticles with size of 100–200 nm in the ternary SiGC composite distribute on the surface of graphite flakes with almost no agglomeration, which is favorable to mitigate the volume change effect of Si particles during the charge/discharge process. As shown in Fig. 3d, the EDS elemental mappings demonstrate that Si nanoparticles distribute in the prepared SiGC homogeneously. However, Si nanoparticles in the binary SiG (see Fig. S2c), without being coated by the sucrose-derived amorphous carbon, agglomerate severely. The nanostructure of the SiGC composite is further identified in the TEM image (Fig. 3e and f). It can be seen that Si nanoparticles dispersed evenly on crystal graphite substrate are coverd by slightly wrinkled graphene-like thin film which is the amorphous cabon derived from sucrose. From

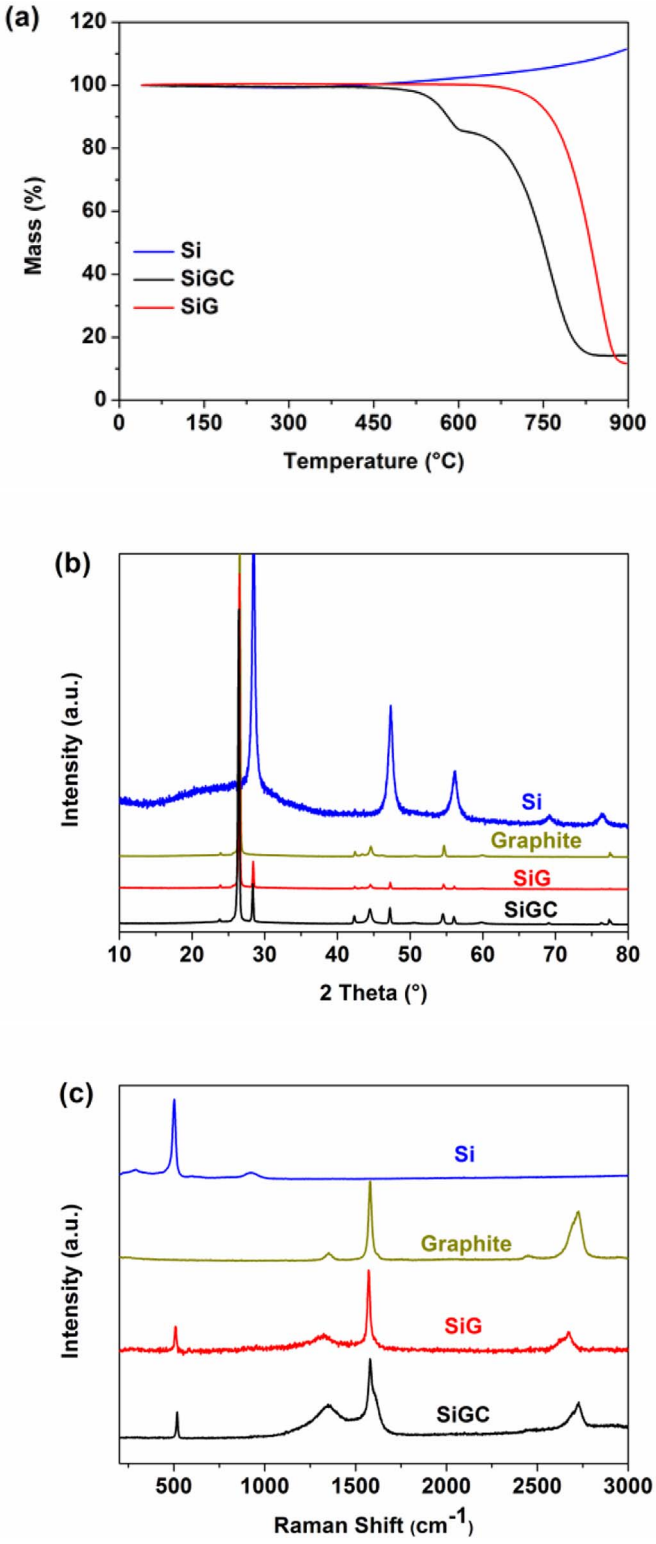

Fig. 2. (a) TG analysis of ball-milled Si, SiG and SiGC in air with a heating rate of 10 °C min^{-1}; (b) XRD patterns and (c) Raman spectra of ball-milled Si, pristine graphite, SiG and SiGC.

high resolution transmission electron microscope image, distinct lattice fringes with spacing of 0.313 nm and 0.336 nm are observed, which correspond to the (111) plane of Si and the (002) plane of the graphite, respectively. It is obvious that the amorphous carbon shell effectively constructs a protecting layer enwrapping the Si nanoparticles and could accommodate the volume change of Si during charge/discharge

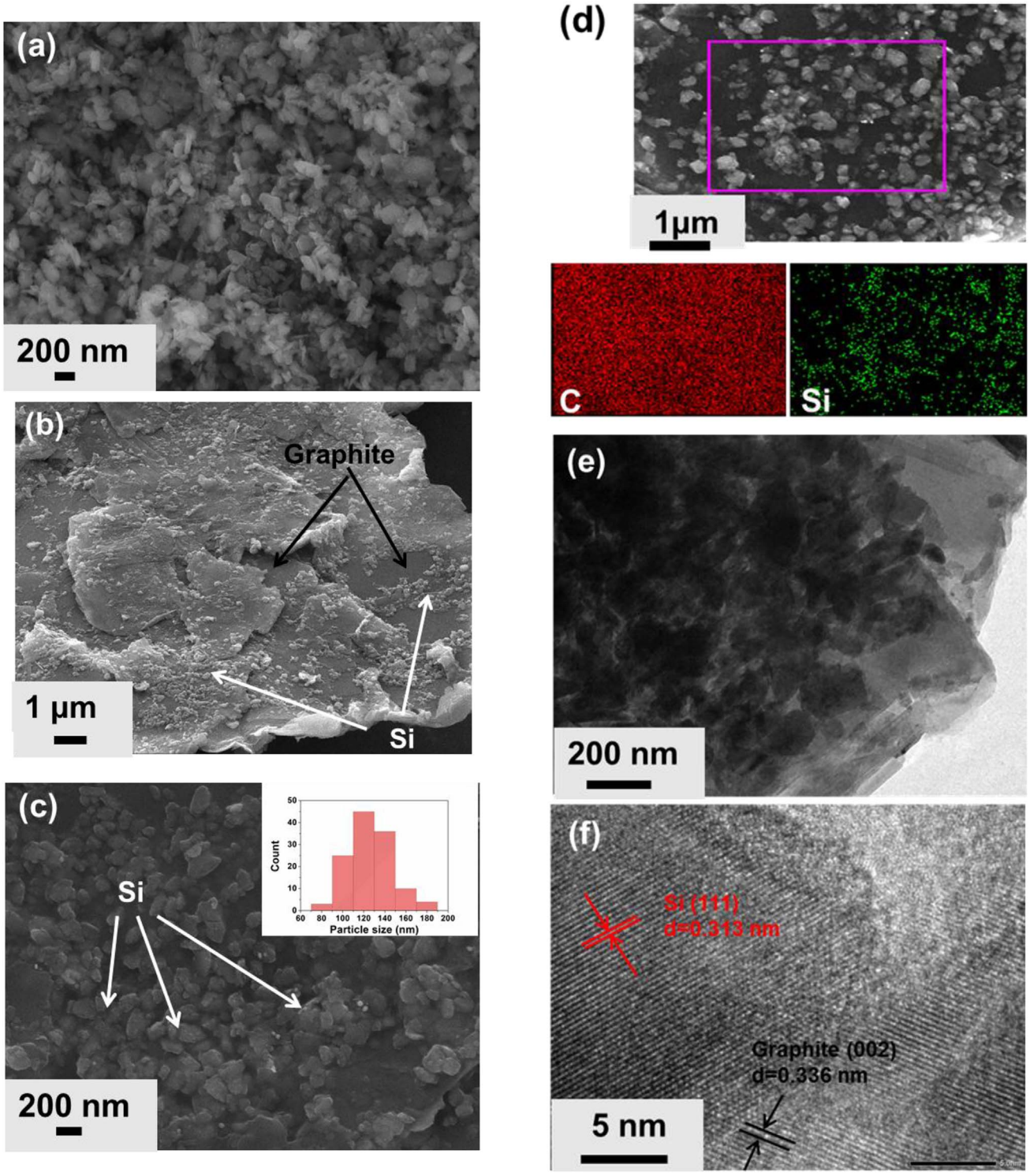

Fig. 3. SEM images of (a) ball-milled Si, (b) and (c) the SiGC composite (inset: the size distribution of Si nanoparticles); (d) EDS elemental mappings of SiGC composite; (e) TEM and (f) HRTEM images of the SiGC composite.

process. The above results also indicate that the amorphous carbon shell might also work as an adhesive agent. Therefore, the ternery SiGC composite with a structure of crystal core and amorphous shell would be expected to show a promissing electrochemical performance as anode material for LIBs [12].

3.2. Electrochemical performance

The galvanostatic charge/discharge profiles of the SiGC with different starting mass ratios (1:4:5, 1:7:5, 1:10:5), SiG, and ball-milled nano-Si during the first two cycles at 0.1 A g^{-1} were investigated and shown in Fig. 4a and Fig. S3. Compared with SiGC (1:4:5) and SiGC (1:10:5), SiGC (1:7:5) shows the best performance in terms of the specific capacity and rate capability, which can be ascribed to the proper starting mass ratio of Si, graphite and sugar. SiGC (1:4:5) shows relatively high specific capacity but unsatisfied rate performance because of its higher Si content, while SiGC (1:10:5) shows good rate capability but low specific capacity. As a result, we chose SiGC (1:7:5)

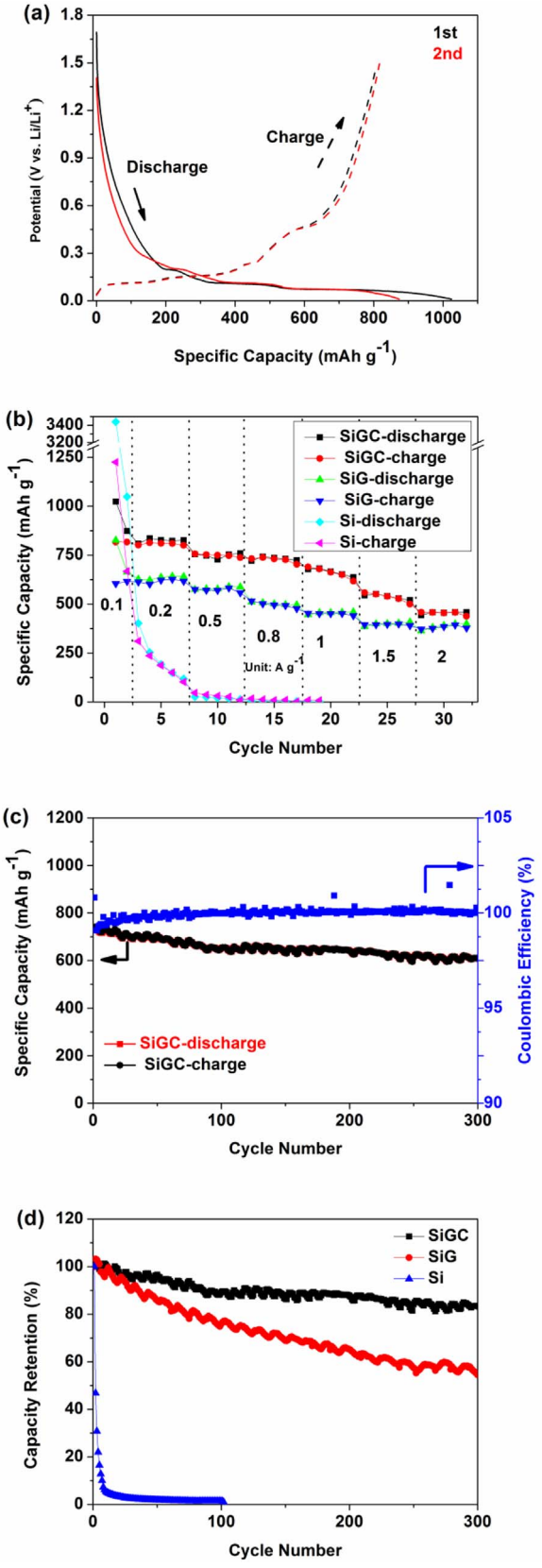

Fig. 4. (a) The galvanostatic charge/discharge profiles of SiGC for the first two cycles at a current density of 0.1 A g^{-1}; (b) rate capabilities of ball-milled Si, SiG and SiGC; (c) cycling performance of SiGC for 300 cycles at 0.5 A g^{-1}; (d) capacity retention of ball-milled Si, SiG and SiGC at 0.5 A g^{-1}.

as the optimized sample for further electrochemical performance investigation. The ball-milled Si nanoparticle without introducing any carbon component shows the worst performance (Fig. S4a). Despite its super high first discharge capacity of 3439 mAh g^{-1}, its first charge capacity is only 1225 mAh g^{-1} with initial CE as low as 35.6%. Moreover, the discharge and charge capacity decays rapidly to 1050 mAh g^{-1} and 668 mAh g^{-1} in the second cycle with CE of only 63.7%. This large irreversible capacity and low CE can be ascribed to volume change effect, resulting in architectural pulverization and constant formation of SEI [13]. For the binary SiG composite (Fig. S4b), it shows improved initial CE (72.2%) and moderate reversible capacity (~600 mAh g^{-1}) because of the introduction of crystal graphite core to act as a conducting supporter for Si nanoparticles. By incorporating SiG with the second carbon phase of amorphous shell, the ternary SiGC composite shows much better performance in term of capacity stability and initial CE. SiGC delivers a maximum discharge capacity of 1016 mAh g^{-1} and charge capacity of 818 mAh g^{-1} with initial CE of 80.5% in the first cycle and shows no capacity degradation in the second cycle. Compared to SiG and ball-milled Si, both the CE and reversible capacity of SiGC are much enhanced, indicating high reversibility of lithium alloy and de-alloy [12]. The super performance of SiGC should be ascribed to the core/shell structured ternary composite. In detail, the crystal core of graphite provides a stable and highly conductive supporter for Si and the amorphous shell of pyrolytic carbon accounts for high CE by keeping the integrity of the electrode and also decreasing side reactions.

The rate performance of SiGC, SiG and ball-milled Si nanoparticles is compared in the current density range of 0.1–2 A g^{-1}. As illustrated in Fig. 4b, the ternary composite with structure of crystal core and amorphous shell endows it to have higher reversible capacity than binary SiG. In Fig. 4b and Fig. S5, the reversible capacity of SiGC is 817, 810, 756, 738, 690, and 558 mAh g^{-1} at 0.1, 0.2, 0.5, 0.8, 1, and 1.5 A g^{-1}, respectively. Even at a high current density of 2 A g^{-1}, SiGC was able to deliver a high specific capacity of 458 mAh g^{-1} which is still higher than that of SiG (~370 mAh g^{-1} at 2 A g^{-1}) and commercially used graphite. On the contrary, the capacity of ball-milled Si became neglectable when just enhancing the current density to 0.5A/g. Such excellent rate performance of SiGC is due to the peculiar crystal core and amorphous shell structure, which is supposed to enhance the electron and ion conductivity of the composite [14].

Furthermore, the cycling performance of SiGC, SiG and ball-milled Si were examined. As shown in Fig. 4c and d and Fig. S6, we can see that SiGC shows much better cycling stability than SiG and pure Si nanoparticles. SiGC displays high reversible capacity of 736 mAh g^{-1} at 0.5 A g^{-1} after two activation cycles at 0.1 A g^{-1} and exhibits excellent stability over 300 cycles. It should be noted that SiGC still delivers a high capacity of 610 mAh g^{-1} (capacity retention of 83.6%) after 300 cycles with only 0.054% average capacity loss per cycle, which is much better than the similar studies in literature [29,30]. The CE of SiGC stabilizes at nearly 100% in the whole 300 cycles, indicating that a super stable SEI was formed. By contrast, the capacity of SiG decreased dramatically from 571 mAh g^{-1} to only 310 mAh g^{-1} (capacity retention of 54.3%) after 300 cycles and ball-milled Si can only survived for several cycles with even low and unstable CE. The excellent cycling result of SiGC derives from the ternary composite with a structure of crystal core and amorphous shell, which accommodates the volume variation of Si particles, as well as promotes the stable formation of SEI. Furthermore, the amorphous carbon shell reinforces the contact between active materials and current collector, thus maintaining the integrity of the electrode [12,31].

EIS measurements were conducted on ball-milled Si, SiG, and SiGC before and after cycling to further investigate the superior electrochemical performance of SiGC. As observed in the Nyquist plots of Fig. 5a, all the three samples show a compressed semicircle in the high-frequency region and an inclined line in the low-frequency region, which can be assigned to the charge-transfer resistance and semi-

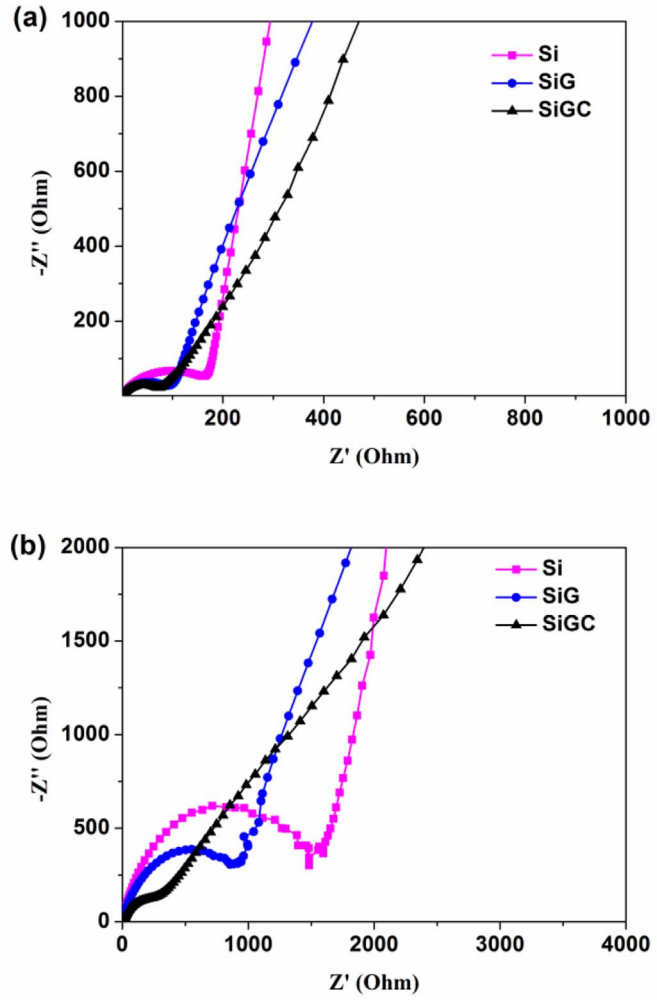

Fig. 5. Electrochemical impedance spectra of ball-milled Si, SiG and SiGC before (a) and after (b) cycling.

diffusion of lithium ions respectively [12,32]. SiGC displays smaller diameters of the semicircles (means smaller impedance resistance) compared to SiG and pure ball-milled Si, indicating a decreased charge-transfer resistance which is due to the crystal graphite core and amorphous carbon shell structure to increase both electron and ion conductivity. After cycling, the resistance of SiGC is still much lower than that of Si and SiG (Fig. 5b). This result consists with the above-mentioned electrochemical performances and thus proves the advantages of the ternary structure of SiGC with crystal core and amorphous shell.

4. Conclusion

By using an industrial applied approach of ball-milling, spray-drying and thermal pyrolysis, we developed a high-performance ternary Si/graphite/pyrolytic carbon anode material with a structure of crystal graphite core and amorphous carbon shell using low-cost materials. The novel core/shell structure not only provided a supporter and highly conductive matrix for Si but also accommodated the volume change effect during charge/discharge. In addition, the amorphous carbon shell keeps the integrity of the composite architecture and solves the silicon related problems of architectural pulverization, contact loss between active material and current collector, and constant formation of SEI. Compared with binary SiG, SiGC with a core/shell structure demonstrates the best electrochemical performances in terms of reversible specific capacity, initial CE, rate capability and cycling stability. SiGC has commercially acceptable high reversible capacity of 818 mAh g^{-1} at 0.1 A g^{-1} with initial CE over 80% and good rate capability (756 and 458 mAh g^{-1} for 0.5 and 2 A g^{-1}, respectively). More importantly, the SiGC also displays excellent cycling stability with capacity retention of 610 mAh g^{-1} (83.6%) after 300 cycles at 0.5 A g^{-1}. These results indicate that this ternary material might offer a competitive choice for a potential Si-based anode material for commercial and practical application in LIBs.

Acknowledgements

This work was supported by the Ministry of Science and Technology of China (2016YFA0200200), the National Natural Science Foundation of China (51633002, 51472124, and 21421001), 111 Project (B12015), and Tianjin city (16ZXCLGX00100).

Appendix A. Supplementary data

Supplementary data related to this article can be found at http://dx.doi.org/10.1016/j.jpowsour.2018.03.008.

References

[1] B. Scrosati, J. Hassoun, Y.K. Sun, Energy Environ. Sci. 4 (2011) 3287–3295.
[2] N. Nitta, F. Wu, J.T. Lee, G. Yushin, Mater. Today 18 (2015) 252–264.
[3] M. Armand, J.M. Tarascon, Nature 451 (2008) 652–657.
[4] J.W. Fergus, J. Power. Sources 195 (2010) 939–954.
[5] C.-M. Park, J.-H. Kim, H. Kim, H.-J. Sohn, Chem. Soc. Rev. 39 (2010) 3115–3141.
[6] M.N. Obrovac, L. Christensen, Electrochem. Solid State Lett. 7 (2004) A93–A96.
[7] A. Magasinski, P. Dixon, B. Hertzberg, A. Kvit, J. Ayala, G. Yushin, Nat. Mater. 9 (2010) 353–358.
[8] J.R. Szczech, S. Jin, Energy Environ. Sci. 4 (2011) 56–72.
[9] C.K. Chan, H. Peng, G. Liu, K. McIlwrath, X.F. Zhang, R.A. Huggins, Y. Cui, Nat. Nanotechnol. 3 (2008) 31–35.
[10] Z.-J. Han, N. Yabuuchi, K. Shimomura, M. Murase, H. Yui, S. Komaba, Energy Environ. Sci. 5 (2012) 9014–9020.
[11] M.-Q. Li, M.-Z. Qu, X.-Y. He, Z.-L. Yu, Electrochim. Acta 54 (2009) 4506–4513.
[12] F. Zhang, X. Yang, Y. Xie, N. Yi, Y. Huang, Y. Chen, Carbon 82 (2015) 161–167.
[13] H. Wu, Y. Cui, Nano Today 7 (2012) 414–429.
[14] C. Ma, C. Ma, J. Wang, H. Wang, J. Shi, Y. Song, Q. Guo, L. Liu, Carbon 72 (2014) 38–46.
[15] L.-F. Cui, Y. Yang, C.-M. Hsu, Y. Cui, Nano Lett. 9 (2009) 3370–3374.
[16] S. Jeong, J.-P. Lee, M. Ko, G. Kim, S. Park, J. Cho, Nano Lett. 13 (2013) 3403–3407.
[17] H. Kim, B. Han, J. Choo, J. Cho, Angew. Chem. Int. Ed. 47 (2008) 10151–10154.
[18] C.K. Chan, R.N. Patel, M.J. O'Connell, B.A. Korgel, Y. Cui, ACS Nano 4 (2010) 1443–1450.
[19] J.-K. Yoo, J. Kim, Y.S. Jung, K. Kang, Adv. Mater. 24 (2012) 5452–5456.
[20] X. Liu, Z. Wang, H. Guo, X. Li, R. Zhou, Y. Zhou, Ionics 23 (2017) 2311–2318.
[21] H. Chen, Z. Wang, X. Hou, L. Fu, S. Wang, X. Hu, H. Qin, Y. Wu, Q. Ru, X. Liu, S. Hu, Electrochim. Acta 249 (2017) 113–121.
[22] Q. Xu, J.-Y. Li, J.-K. Sun, Y.-X. Yin, L.-J. Wan, Y.-G. Guo, Adv. Energy Mater. 7 (2017) 1601481.
[23] X. Han, H. Chen, J. Liu, H. Liu, P. Wang, K. Huang, C. Li, S. Chen, Y. Yang, Electrochim. Acta 156 (2015) 11–19.
[24] H. Li, C. Lu, B. Zhang, Electrochim. Acta 120 (2014) 96–101.
[25] L. Gan, H. Guo, Z. Wang, X. Li, W. Peng, J. Wang, S. Huang, M. Su, Electrochim. Acta 104 (2013) 117–123.
[26] S. Jeong, X. Li, J. Zheng, P. Yan, R. Cao, H.J. Jung, C. Wang, J. Liu, J.-G. Zhang, J. Power Sources 329 (2016) 323–329.
[27] M. Li, X. Hou, Y. Sha, J. Wang, S. Hu, X. Liu, Z. Shao, J. Power Sources 248 (2014) 721–728.
[28] M. Su, Z. Wang, H. Guo, X. Li, S. Huang, W. Xiao, L. Gan, Electrochim. Acta 116 (2014) 230–236.
[29] R. Zhou, H. Guo, Y. Yang, Z. Wang, X. Li, Y. Zhou, J. Alloys Compd. 689 (2016) 130–137.
[30] S.S. Hwang, C.G. Cho, H. Kim, Electrochim. Acta 55 (2010) 3236–3239.
[31] T. Zhang, J. Gao, L.J. Fu, L.C. Yang, Y.P. Wu, H.Q. Wu, J. Mater. Chem. 17 (2007) 1321–1325.
[32] S. Yang, G. Li, Q. Zhu, Q. Pan, J. Mater. Chem. 22 (2012) 3420.